Available online at www.sciencedirect.com
ScienceDirect
International Journal of Multiphase Flow 32 (2006) 1182–1190
International Journal of Multiphase Flow
www.elsevier.com/locate/ijmulflow

Effect of gas expansion on the velocity of a Taylor bubble: PIV measurements

R.G. Sousa, A.M.F.R. Pinto, J.B.L.M. Campos *

Centro de Estudos de Fenómenos de Transporte, Departamento de Engenharia Química, Faculdade de Engenharia da Universidade do Porto, Rua Dr. Roberto Frias 4200-465 Porto, Portugal

Received 23 January 2006; received in revised form 4 June 2006

Abstract

The effect of gas expansion on the velocity of a Taylor bubble was studied experimentally. The velocity field in the liquid ahead of a Taylor bubble was measured by particle image velocimetry (PIV), and the bubble velocity was measured with two pairs of laser diodes and photocells. The experiments were done in a 7.0 m long vertical tube with a 32 mm internal diameter. Solutions of carboxymethylcellulose (CMC) polymer with weight percentages between 0.01% and 0.1% were used. The expansion of slug gas induces an increase in the bubble velocity and a corresponding displacement of the liquid ahead of the bubble. The velocity of the bubble increases by an amount equal to the maximum velocity in the liquid displaced. For the solutions studied, the induced velocity profile was parabolic and the bubble velocity increase was equal to the liquid velocity at the tube axis, i.e., twice the mean velocity in the liquid displaced. The corrected velocity obtained by subtracting the velocity increase from the value of the bubble velocity is independent of the bubble length.

Keywords: Taylor bubble; Taylor bubble expansion; Taylor bubble velocity; PIV measurements

1. Introduction

Large gas bubbles rising in vertical tubes of liquid have an elongated shape and are commonly called Taylor bubbles or gas slugs. Over the years several studies have been published about the hydrodynamics of Taylor bubbles rising in stagnant and co-current liquids. These studies are mainly about the rise velocity and flow field around the Taylor bubbles. Dumitrescu (1943), and later Davies and Taylor (1950), applied potential flow theory to flow around the bubble nose to find that the drift velocity of an elongated bubble, U_0 rising in a vertical column filled with stagnant water is given by

$$U_0 = k\sqrt{gD} \tag{1}$$

* Corresponding author. Fax: +351 225 08 1449.
E-mail address: jmc@fe.up.pt (J.B.L.M. Campos).

0301-9322/$ - see front matter
doi:10.1016/j.ijmultiphaseflow.2006.06.002

where g is the gravity acceleration, D the column internal diameter and k a dimensionless constant. For inertia-controlled regime, where the fluid can be considered inviscid and surface tension effects negligible, k is found to be around 0.35. Nicklin et al. (1962), experimentally confirmed this value and showed that the velocity of a single Taylor bubble, U_b, rising in a co-current flowing liquid is given by

$$U_b = C \cdot U_s + U_0 \tag{2}$$

where $C \cdot U_s$ is the fluid velocity at the axis of the column ahead of the nose of the bubble and U_s the superficial liquid velocity. The value of C is generally assumed to depend on the velocity profile in the liquid ahead of the bubble and can be seen as the ratio between the maximum to the mean velocity in the profile. According to this, C should be around 2 for laminar liquid flow and 1.2 for turbulent liquid flow. Several experimental studies were carried out to test the relation between the bubble velocity and the velocity profile in the liquid ahead of it. Among these are those done by Shemer and Barnea (1987), Polonsky et al. (1999), Pinto et al. (2005) and Van Hout et al. (2002). These studies covered different flow regimes and applied different techniques, but, in general, the values of the experimental constant C were in agreement with theory. Among more recent studies, those of Nogueira et al. (2006) and Sousa et al. (2004, 2005) employed particle image velocimetry (PIV) to describe the flow field around Taylor bubbles rising in Newtonian and non-Newtonian solutions. The present study is concerned with the effects of continuous gas expansion on bubble velocity and on the liquid velocity ahead/downstream of the bubble. Intuition tells us that the velocity increase is due to gas expansion causing an increased displacement of the bubble nose (the tube is open to the atmosphere at the top and the liquid below the bubble is incompressible). But intuition is not always scientifically accurate and the effect is not so simple to characterise, as we will see. This is a very fundamental study, but, so far as we know, there is no experimental study in the literature which clarifies this effect. The experimental technique used, PIV, will be briefly described in the next section.

2. Experiments

2.1. Experimental technique

The flow field ahead of a single Taylor bubble rising in stagnant liquids was obtained by means of particle image velocimetry (PIV). This technique, as applied to slug flow, is fully described by Nogueira et al. (2003). A PCO (SensiCam) CCD camera (resolution of 1024×1280 pixels^2) and an acquisition and data processing system constitute the basis of the instrumentation. An Nd:YAG laser with 400 mJ of pulse power was used to illuminate the vertical measured plane containing the column axis. The laser wavelength was 532 nm and the pulse duration 2.4 ns. Fluorescent particles (an orange vinyl pigment of 10 μm mean size) were used as seeding, emitting light at 590 nm. A 35 mm lens was used and a red filter, opaque below 550 nm, was placed in front of the PCO CCD camera to block the intense green reflections of the laser but allow passage of the light emitted by the fluorescent particles. The same signal generator triggered both the laser and the video camera. Two laser diodes were positioned close to the vertical column, aimed through the tube axis at two photocells placed on the opposite side. The signal yielded by each photocell is proportional to the laser light received. When the Taylor bubble passes between the laser diode and the photocell, the laser beam is deflected and the photocell signal drops abruptly. The bubble velocity was determined by dividing the distance between the two photocells by the time lag between the corresponding drop of signal.

2.2. Facility

The present study was carried out in the experimental setup schematically shown in Fig. 1 and fully described by Sousa et al. (2004).

The test facility was built around an acrylic tube, 7.0 m in height with an internal diameter of 0.032 m (D) open to the atmosphere on top, and included two pneumatic valves, two storage tanks and a pump. Individual

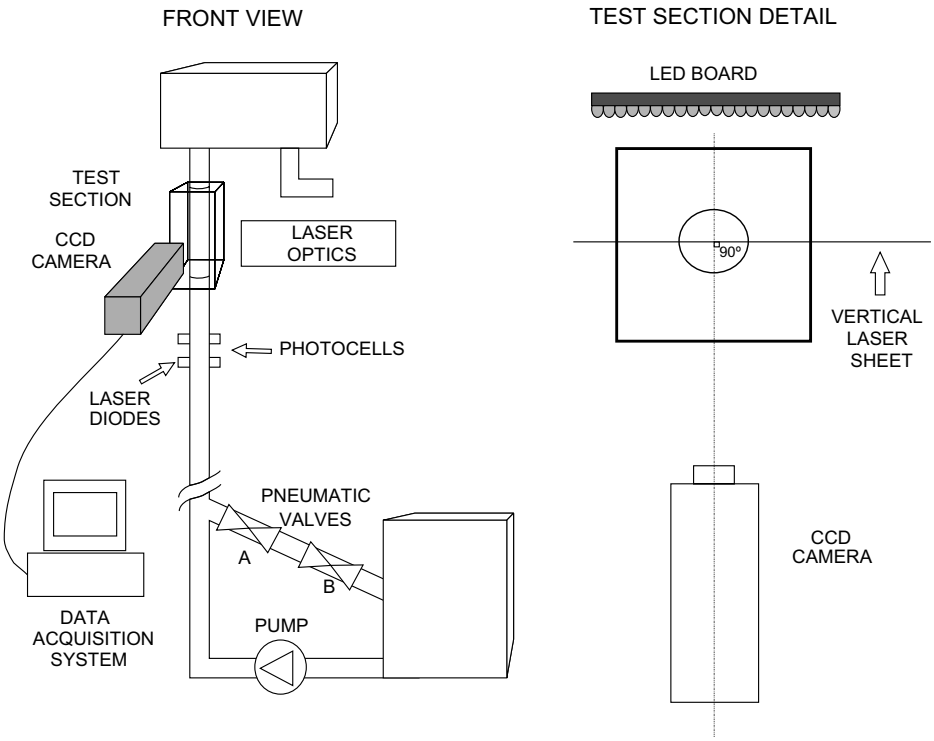

Fig. 1. Schematic representation of the experimental setup and detailed top view of the test section.

Taylor bubbles were injected at the bottom of the column by manipulating valves A and B: opening valve B allows the liquid trapped between the valves to drain back into the reservoir and the space to fill with air; closing valve B and opening valve A releases the air between the valves to rise up in the form of a long Taylor bubble. The bubble volume was controlled by regulating the opening time of valve B. The study focused on bubbles with lengths long enough to assure that a fully-developed liquid film flowed around the bubbles, but not so long as to induce wave instabilities in this liquid film (rippling). The liquid flow field was measured at 4.0 m (125D) above the gas injection, far enough to avoid entrance effects and assure a stabilised flow. A box with plane faces surrounded the test section (0.5 m × 0.12 m × 0.11 m), and to minimise optical distortions

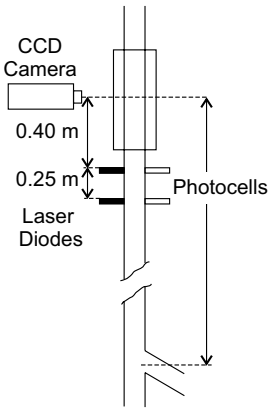

Fig. 2. Distances between photocells, test section and bubble injection system.

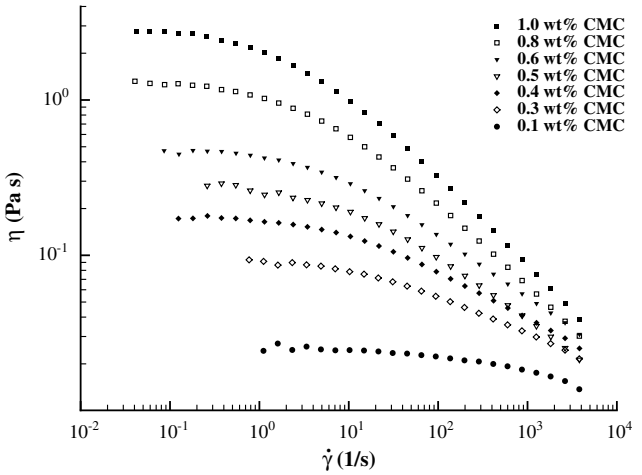

Fig. 3. Viscosity of the CMC solutions studied as a function of the shear rate.

this was filled with the same experiment liquid as was in the column. Two pairs of laser diodes/photocells were mounted perpendicular to the column and 0.25 m apart. The upper diode/photocell was placed 0.40 m (12.5D) below the middle of the flow field test section. Fig. 2 shows these measurement sections and the respective distances.

Two thermocouples, placed above and below the test section, were used to measure the working temperature and detect any possible temperature gradient along the column. The liquids were CMC solutions with different weight percentages. In Fig. 3, the viscosity (η) of the studied solutions is represented as a function of the shear rate ($\dot{\gamma}$).

2.3. Experimental procedure

At the instant when the bubble crossed the middle plane between the photocells, the flow field in the test section was measured by PIV. In this way, both the mean bubble velocity between the two diodes/photocells and the liquid velocity profile/flow rate, approximately 0.50 m (15D) ahead of the bubble nose, were measured simultaneously.

3. Data processing

The processing procedure of the PIV images is fully described in Nogueira et al. (2003). The flow field was obtained using the cross-correlation algorithm WIDIM (Window Displacement Iterative Multigrid), developed by Scarano and Riethmuller (1999). In the present work, initial interrogation windows had 20×40 pixels^2 and, after the first vector estimate, the final windows had 10×20 pixels^2. An interrogation area overlap of 50% and spurious vector identification were used. The vectors with a signal-to-noise ratio of less than 1.5 (about 5–7% of the total vectors) were corrected, taking the average neighbouring value. The liquid velocity ahead of the bubble is very low, and so only large time gaps between PIV images can detect particle displacement. To measure the flow field the first frames of consecutive pairs of PIV images were used, corresponding to a time interval between 500 and 2000 s and a maximum particle displacement of about 5–7 pixels. Tests made with known particle displacements showed a maximum uncertainty of 0.2 pixels, giving a relative error on the liquid velocity of about 4%.

The velocity (U_b) and length (L_b) of the bubbles were determined from the known distance between the photocells, h_{pc}, and the time gap between their signals, as shown in Fig. 4. The relative error in the bubble velocity measured by this method is around 2%, which is higher than the bubble velocity variation between the photocells.

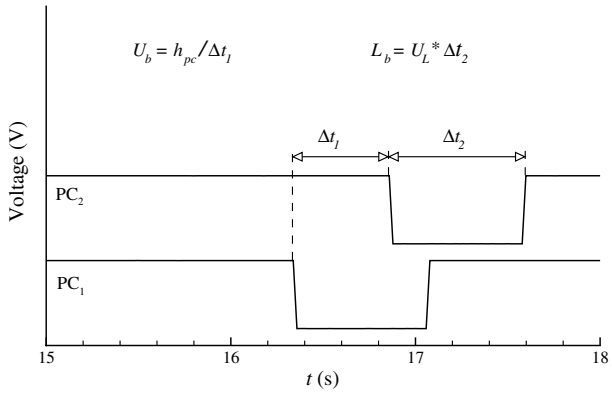

Fig. 4. Signal obtained from the photocells to determine the bubble velocity, U_b, and bubble length, L_b.

4. Experimental results

The experiments used seven aqueous solutions of Carboxymethylcellulose, with a range of polymer weight percentages between 0.1 wt% and 1.0 wt% CMC. Several bubble volumes were used for each solution, varying between $2D$ to $14D$ in length.

4.1. Bubble velocity

During the PIV measurements the column was open to the atmosphere on top. The bubble velocity and the bubble length were measured by the diodes/photocells placed below the test section (Fig. 2). In Fig. 5 the bubble velocity is represented versus the bubble length for the different solutions of CMC.

As expected, bubble velocity depends on the bubble length since the column is open to the atmosphere at the top and the bubbles expand during the rise. The outcome of bubble expansion, resulting in an increase in bubble velocity, is explained in the following section.

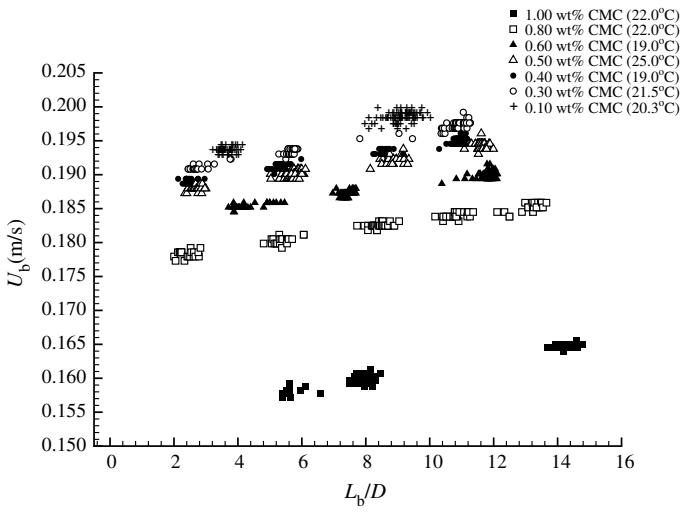

Fig. 5. Bubble velocity versus bubble length for several CMC solutions.

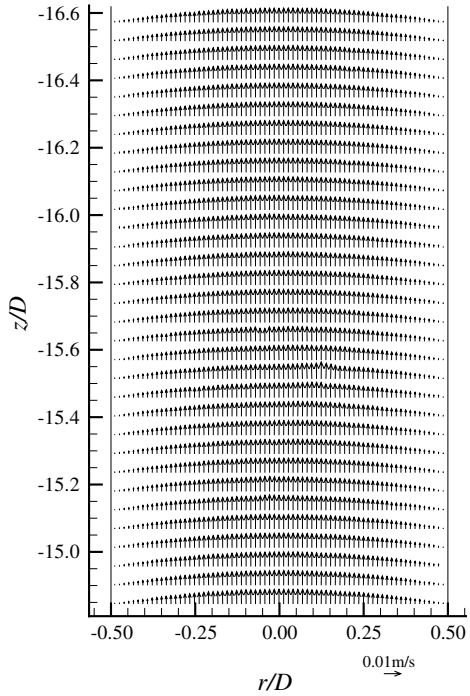

Fig. 6. Flow field ahead of a bubble with 11.7D of length rising in a 0.50 wt% CMC solution.

4.2. Liquid flow in front of the slug bubble

The flow field in the liquid in front of a bubble, 15D–16D ahead of the bubble "nose", is presented in Fig. 6 for a 0.50 wt% CMC solution (the bubble length was 11.7D), where z is the axial distance to the bubble nose and r the radial distance to the axis of the column.

The mean (30 profiles × 30 identical bubbles) liquid velocity (V_z) profiles ahead of the bubbles (for four different bubble lengths) are represented in Fig. 7. From this figure it is clear that the velocity of the liquid ahead of the bubble increases in step with an increasing bubble length. In the flow field the maximum shear rate is

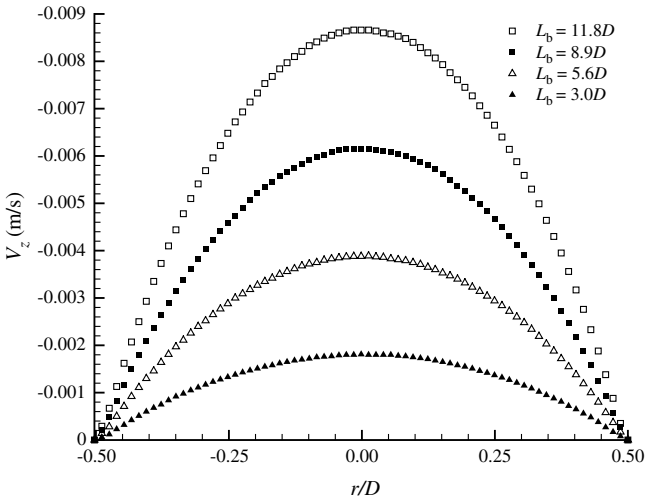

Fig. 7. Liquid velocity profiles in front of bubbles with different length (L_b) rising in a 0.50 wt% CMC solution.

around 1 s^{-1} since the velocity gradients are very low, and so the liquid viscosity is almost uniform (see Fig. 3). Therefore, the CMC solutions behave like a Newtonian fluid in this region. The velocity profiles fall within the same curve (Fig. 8) when they are represented in a dimensionless form, i.e., dividing each velocity by the maximum velocity (at the centre of the column). The comparison between the dimensionless curve and the parabolic profile in a Newtonian fluid is also shown in Fig. 8. Identical curves were obtained for the other CMC solutions.

4.3. Bubble velocity due to gas expansion

The effect of gas expansion on bubble velocity during its rise can be eliminated if the maximum velocity in the liquid profile (at the column axis) is subtracted from the bubble velocity. The values obtained after this correction are plotted in Fig. 9 for the conditions studied. For each fluid a constant bubble velocity is obtained, independent of the bubble length. This constant is the bubble velocity when the column is closed on both ends, thereby preventing any bubble expansion.

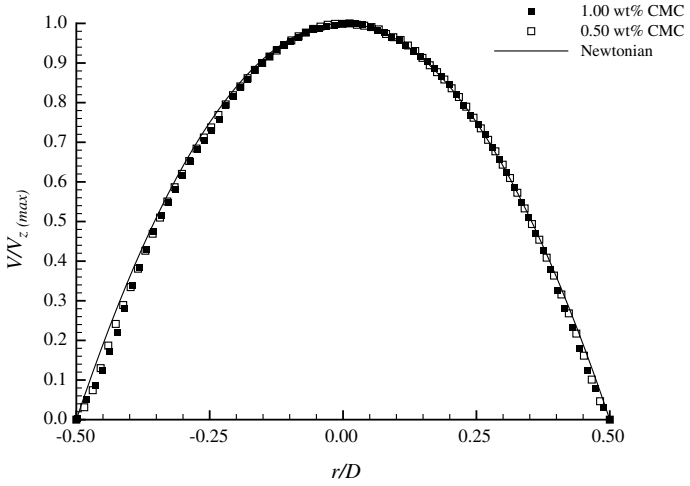

Fig. 8. Comparison between the dimensionless liquid velocity profiles ahead of the bubbles in CMC solutions with the Newtonian laminar profile.

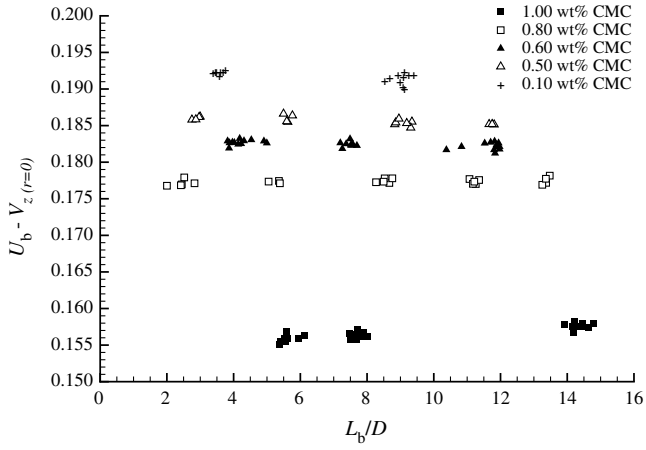

Fig. 9. Bubble velocity versus bubble length, after subtraction of the maximum liquid velocity (at the column axis) ahead of the bubble.

4.4. Relation between volumetric liquid flow rate above the bubble and the volumetric bubble expansion rate

If the liquid ahead of the bubble is in movement due to bubble expansion, the volumetric liquid flow rate above the bubble must be equal to the volumetric bubble expansion rate. The liquid flow rate (Q_{exp}) is obtained integrating the velocity profile across the sectional area of the column.

The volumetric bubble expansion rate can be determined by an alternative method. The static pressure inside the bubble is given by

$$P(h) = P_{atm} + \rho g h \tag{3}$$

where h is the distance between the bubble "nose" and the liquid surface, P_{atm} is atmospheric pressure and ρ is the liquid density. The perfect gas law gives the bubble volume (ϑ_b) at a distance h from the liquid surface as

$$\vartheta_b = \frac{nRT}{P(h)} = \frac{nRT}{P_{atm} + \rho g h} \tag{4}$$

The variation of the bubble volume with h is given by

$$\frac{\partial \vartheta_b}{\partial h} = -\frac{nRT}{(P_{atm} + \rho g h)^2}\rho g = \frac{\vartheta_b}{P_{atm} + \rho g h}\rho g \tag{5}$$

The rate of variation of the bubble volume is

$$\frac{\partial \vartheta_b}{\partial t} = \frac{\partial \vartheta_b}{\partial h}\frac{\partial h}{\partial t} = \frac{\partial \vartheta_b}{\partial h}U_b \tag{6}$$

This rate can be calculated by combining Eqs. (5) and (6), if ϑ_b and h are known. Sousa et al. (2005) presented accurate correlations to determine the entire bubble shape in CMC solutions, with an error below 4%:

$$r_b/D = k_1 \cdot \tanh(k_2 \cdot (z/D)^{k_3}) \tag{7}$$

where, r_b is the bubble radius, z the distance to the bubble nose and D the internal column diameter. k_1, k_2 and k_3 are fitting parameters, which depend on the Reynolds number according to the following equations:

$$k_1 = 0.019\ln(Re) + 0.342 \tag{8}$$

$$k_2 = 3.983 \cdot Re^{-0.111} \tag{9}$$

$$k_3 = 0.648 \cdot Re^{-0.068} \tag{10}$$

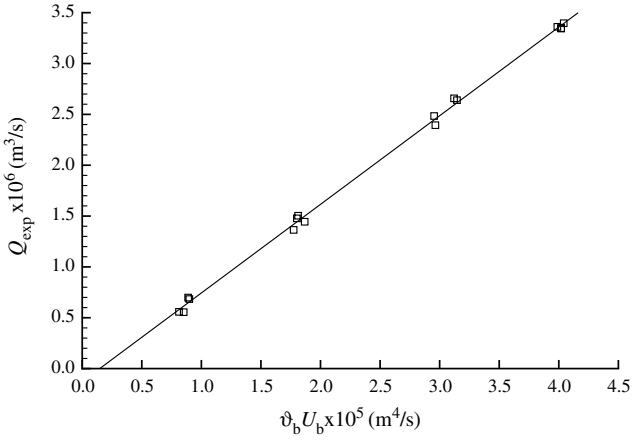

Fig. 10. Experimental liquid flow rates versus $\vartheta_b U_b$ for the 0.5 wt% CMC solution.

Taking these correlations, the bubble volume is determined by integration of infinitesimal volume elements along the bubble length:

$$\vartheta_b = \int_{z=0}^{L_b} \pi r_b^2 \, dz \tag{11}$$

Taking a mean value of 1.6 m for h (the distance from the middle plane between the laser/photocells and the liquid surface) and combining Eqs. (5) and (6) yields:

$$\frac{\partial \vartheta_b}{\partial t} = \frac{\rho g}{P_{atm} + \rho g h} \vartheta_b U_b = 0.084 \vartheta_b U_b \tag{12}$$

Fig. 10 shows the experimental liquid flow rate in front of the bubble versus $\vartheta_b U_b$ (0.5 wt% CMC solution). The liquid flow rate varies linearly with $\vartheta_b U_b$, being the slope 0.087 m^{-1}, not far from 0.084 m^{-1} predicted by Eq. (12). At the origin the ordinate has a very small value: -1.2×10^{-7} m^3 s^{-1}.

5. Conclusions

The effect of gas expansion on Taylor bubble velocity was experimentally studied using particle image velocimetry (PIV). The main conclusions of this work, based on accurate experimental data are

- Bubble expansion during the rise induces a continuous displacement of the liquid ahead.
- The bubble velocity increase due to the gas expansion is equal to the maximum velocity in the liquid displaced ahead of it.
- If the previous contribution to the total bubble velocity is subtracted, the corrected value of the bubble velocity becomes independent of the bubble length.

Acknowledgements

The authors acknowledge the financial support given by F.C.T., SFRH/BD/3389/2000. This work was also supported, via CEFT, by POCTI (FEDER).

References

Davies, R.M., Taylor, G.I., 1950. The mechanics of large bubbles rising through extended liquids and through liquid tubes. Proc. R. Soc. London Ser. A 200, 375–390.

Dumitrescu, D.T., 1943. Strömung an einer luftblase im senkrechten rohr. Z. Angew. Math. Mech. 23, 139.

Nicklin, D.J., Wilkes, J.O., Davidson, J.F., 1962. Two-phase flow in vertical tubes. Trans. Inst. Chem. Engrs. 40, 61.

Nogueira, S., Sousa, R.G., Pinto, A.M.F.R., Riethmuller, M.L., Campos, J.B.L.M., 2003. Simultaneous PIV and shadowgraphy in slug flow: a solution for optical problems. Exper. Fluids 35, 598–609.

Nogueira, S., Riethmuller, M.L., Campos, J.B.L.M., Pinto, A.M.F.R., 2006. Flow in the nose region and in the annular film around a Taylor bubble rising through vertical columns of stagnant and flowing Newtonian liquids. Chem. Eng. Sci. 61, 845–857.

Pinto, A.M.F.R., Pinheiro, M.N.C., Nogueira, S., Ferreira, V.D., Campos, J.B.L.M., 2005. Experimental study on the transition in the velocity of Taylor bubbles in vertical upward two-phase slug flow. Chem. Eng. Res. Des. 83, 1103–1110.

Polonsky, S., Shemer, L., Barnea, D., 1999. The relation between the Taylor bubble motion and the velocity field ahead of it. Int. J. Multiphase Flow 25, 957–975.

Scarano, F., Riethmuller, M.L., 1999. Iterative multigrid approach in PIV image processing with discrete window offset. Exper. Fluids 26, 513–523.

Shemer, L., Barnea, D., 1987. Visualization of the instantaneous velocity profiles in gas–liquid slug flow. PhysicoChem. Hydrodynam. 8, 243–253.

Sousa, R.G., Nogueira, S., Pinto, A.M.F.R., Riethmuller, M.L., Campos, J.B.L.M., 2004. Flow in the negative wake of a Taylor bubble rising in viscoelastic carboxymethylcellulose solutions: particle image velocimetry measurements. J. Fluid Mech. 511, 217–236.

Sousa, R., Riethmuller, M.L., Pinto, A.M.F.R., Campos, J.B.L.M., 2005. Flow around individual Taylor bubbles rising in stagnant CMC solutions: PIV measurements. Chem. Eng. Sci. 60, 1859–1873.

Van Hout, R., Barnea, D., Shemer, L., 2002. Translational velocities of elongated bubbles in continuous slug flow. Int. J. Multiphase Flow 28, 1333–1350.